AGU PUBLICATIONS

JGR

Journal of Geophysical Research: Atmospheres

RESEARCH ARTICLE

10.1002/2016JD025360

Key Points:
- microphysical and optical properties of stratiform liquid water clouds
- impact of air mass transport on cloud properties
- cloud characterization using a large data set

Correspondence to:
J. Preißler,
jana.preissler@nuigalway.ie

Citation:
Preißler, J., G. Martucci, G. Saponaro, J. Ovadnevaite, A. Vaishya, P. Kolmonen, D. Ceburnis, L. Sogacheva, G. de Leeuw, and C. O'Dowd (2016), Six years of surface remote sensing of stratiform warm clouds in marine and continental air over Mace Head, Ireland, *J. Geophys. Res. Atmos.*, *121*, doi:10.1002/2016JD025360.

Received 13 MAY 2016
Accepted 15 NOV 2016
Accepted article online 22 NOV 2016

Six years of surface remote sensing of stratiform warm clouds in marine and continental air over Mace Head, Ireland

Jana Preißler[1], Giovanni Martucci[2], Giulia Saponaro[3], Jurgita Ovadnevaite[1], Aditya Vaishya[4], Pekka Kolmonen[3], Darius Ceburnis[1], Larisa Sogacheva[3], Gerrit de Leeuw[3], and Colin O'Dowd[1]

[1]Centre for Climate and Air Pollution Studies, National University of Ireland Galway, Galway, Ireland, [2]Federal Office of Meteorology and Climatology MeteoSwiss, Ch. De l'Aérologie, Payerne, Switzerland, [3]Climate Research Unit, Finnish Meteorological Institute, Helsinki, Finland, [4]Space Physics Laboratory, Vikram Sarabhai Space Centre, Thumba, India

Abstract A total of 118 stratiform water clouds were observed by ground-based remote sensing instruments at the Mace Head Atmospheric Research Station on the west coast of Ireland from 2009 to 2015. Microphysical and optical characteristics of these clouds were studied as well as the impact of aerosols on these properties. Microphysical and optical cloud properties were derived using the algorithm SYRSOC (SYnergistic Remote Sensing Of Clouds). Ground-based in situ measurements of aerosol concentrations and the transport path of air masses at cloud level were investigated as well. The cloud properties were studied in dependence of the prevailing air mass at cloud level and season. We found higher cloud droplet number concentrations (CDNC) and smaller effective radii (r_{eff}) with greater pollution. Median CDNC ranged from 60 cm^{-3} in marine air masses to 160 cm^{-3} in continental air. Median r_{eff} ranged from 8 µm in polluted conditions to 10 µm in marine air. Effective droplet size distributions were broader in marine than in continental cases. Cloud optical thickness (COT) and albedo were lower in cleaner air masses and higher in more polluted conditions, with medians ranging from 2.1 to 4.9 and 0.22 to 0.39, respectively. However, calculation of COT and albedo was strongly affected by liquid water path (LWP) and departure from adiabatic conditions. A comparison of SYRSOC results with MODIS (Moderate-Resolution Imaging Spectroradiometer) observations showed large differences for LWP and COT but good agreement for r_{eff} with a linear fit with slope near 1 and offset of −1 µm.

1. Introduction

Besides directly absorbing and scattering sunlight, aerosols also have an indirect effect on the global radiation budget by altering cloud properties. Twomey first proposed an influence of aerosols on cloud albedo by increasing cloud droplet number concentration (CDNC) and consequently reducing droplet sizes [*Twomey*, 1974, 1977]. Besides this, there are other interactions between aerosols and clouds. For example, aerosols can alter cloud lifetime [*Albrecht*, 1989], cloud water content [*Coakley and Angevine*, 2002], and droplet size distribution [*Vong and Covert*, 1998].

According to the Fifth Assessment Report of the Intergovernmental Panel on Climate Change, the physical basis of the albedo effect introduced by Twomey is fairly well understood [*Boucher et al.*, 2013]. However, uncertainties still remain considering the lifetime effect and the shape of the droplet size distribution [*Brenguier et al.*, 2011; *Boucher et al.*, 2013]. *Brenguier et al.* [2003] confirmed the expectations of *Twomey* [1977] of a negative correlation between cloud optical thickness (COT) and cloud droplet effective radius (r_{eff}). Strongly polluted clouds, however, had a positive correlation. In general, r_{eff} of cloud droplets is smaller in clouds affected by polluted air masses than in clean clouds [*Lohmann and Feichter*, 2005, and references therein]. This effect was also observed by *Ferek et al.* [2000] investigating marine clouds influenced by ship emissions. They also found drizzle suppression in ship tracks. *Rosenfeld et al.* [2008] discussed the role of aerosols as cloud condensation nuclei (CCN) and their ambivalent impact on precipitation: on one hand, evaporation or prevention of clouds in heavily polluted conditions, and on the other hand, prevention of long-lived clouds in the tropics due to clean conditions and fast rain out. A review of publications discussing marine and continental stratiform clouds was done by *Miles et al.* [2000]. They found clear differences between these two types in terms of total CDNC, effective diameter, liquid water content (LWC), among others.

For continuous vertically resolved observations of the atmosphere, ground-based remote sensing is advantageous. Better spatial coverage can be achieved by satellite-borne sensors such as the cloud profiling radar on CloudSat [*Stephens et al.*, 2002] or the aerosol lidar CALIOP (Cloud Aerosol Lidar with Orthogonal Polarization) [*Winker et al.*, 2007] on CALIPSO (Cloud-Aerosol Lidar and Infrared Pathfinder Satellite Observations) but at the expense of temporal resolution. Ground-based remote sensing offers continuous monitoring of the atmosphere at one location, with high vertical and temporal resolution. This gives valuable detailed insights into highly complex cloud processes.

Mace Head, located at the west coast of Ireland, receives clean air masses at ground level from a wide sector to the west and polluted air from other sectors [*Jennings et al.*, 2003; *O'Connor et al.*, 2008]. Numerous studies of in situ observations at Mace Head have been published, many addressing marine aerosol [*Ovadnevaite et al.*, 2012; *Ceburnis et al.*, 2014], including CCN [*Reade et al.*, 2006]. *Jennings et al.* [1997] focussed on the characterization of marine and continental aerosols and found lowest aerosol number concentration for polar marine air masses and highest for continental air masses.

The remote sensing suite at Mace Head has previously been used to study clouds. For example, *Martucci et al.* [2010] compared cloud base heights from different colocated ceilometers. Furthermore, the algorithm SYRSOC (SYnergistic Remote Sensing Of Clouds) was developed to provide microphysical cloud properties from data obtained by ceilometer, cloud radar, and microwave radiometer [*Martucci and O'Dowd*, 2011]. This retrieval algorithm was also used for the investigation of the impact of volcanic aerosol and sea spray on clouds (*Martucci et al.* [2012] and *Ovadnevaite et al.* [2011], respectively). Besides, remote sensing data from Mace Head was used in combination with ground-based and airborne in situ measurements [*Dall'Osto et al.*, 2010 and *Martucci et al.*, 2013, respectively). These studies focused on limited time periods. What is missing are long-term cloud observations, their microphysical, and optical properties and the impact of aerosols upon them. The present study provides more than 6 years of ground-based cloud remote sensing at Mace Head. It aims to underpin findings from single case studies or intensive campaigns by using a large data set of carefully selected cloud cases from continuous measurements.

2. Instruments and Methodology

The remote sensing division at Mace Head (53.33°N, 9.90°W) is located 21 m above sea level, about 300 m from the water line. It has been a Cloudnet station [*Illingworth et al.*, 2007] since 2009 and comprises a cloud radar, a ceilometer, and a microwave radiometer (MWR). The radar is a MIRA36, a 35.5 GHz Ka-band Doppler cloud radar from Metek [*Bauer-Pfundstein and Goersdorf*, 2007; *Melchionna et al.*, 2008], which measures in-cloud reflectivity, linear depolarization ratio, and vertical velocity at vertical and temporal resolutions of 30 m and 10 s. The radar was also used to detect cloud top altitude. A calibration offset of the radar reflectivity due to finite receiver loss [*Probert-Jones*, 1962] was taken into account by adding 2 dBZ to the radar reflectivity output (M. Bauer-Pfundstein, METEK, personal communication, 2016). The ceilometer is a CHM15k from Lufft (formerly Jenoptik) [*Heese et al.*, 2010; *Martucci et al.*, 2010] measuring at 1064 nm. It detects photons backscattered from atmospheric targets such as cloud droplets or aerosol particles at vertical and temporal resolutions of 15 m and 30 s. It is capable of detecting aerosol layers, as well as clouds up to a certain penetration depth depending on the cloud optical depth. The ceilometer was used to detect cloud base altitude. The MWR is an RPG-HATPRO [*Crewell and Löhnert*, 2003; *Löhnert and Crewell*, 2003; *Löhnert et al.*, 2009] water vapor and oxygen multichannel microwave profiler [*Martucci and O'Dowd*, 2011]. SYRSOC uses temperature profiles and liquid water path (LWP) from MWR. MWR profiles have a decreasing vertical resolution with range and a temporal resolution of about 15 s. LWP was obtained by quadratic regression retrieval based on brightness temperatures.

This set of instruments enables vertically resolved determination of microphysical cloud properties such as CDNC, r_{eff}, and LWC from the ground. The SYRSOC algorithm was used to retrieve these microphysical cloud properties as well as cloud optical properties, i.e., cloud optical thickness (COT) and cloud albedo. SYRSOC works under the assumptions of a monomodal droplet size distribution with constant shape parameters of 8 (marine and marine-modified clouds) and 9 (continental and continental-modified clouds) [*Miles et al.*, 2000], and uses an explicit subadiabaticity scheme. SYRSOC was described in detail by *Martucci and O'Dowd* [2011], but unlike the outline in this first publication, CDNC in the present work was obtained using radar reflectivity following the approach of *Brandau et al.* [2010] solving equation (5) therein for CDNC, $N(h)$

$$N(h) = k_6 \left(\frac{6\rho_{\text{air}} A_{\text{ad}}}{\pi \rho_w}^2 \frac{1}{Z(h)} f^2(h) h^2 \right), \tag{1}$$

with the constant coefficient k_6 depending on the shape parameter of the droplet-size distribution [*Brandau et al.*, 2010, equation (19)], the density of air, ρ_{air}, the adiabatic lapse rate of LWC mixing ratio, A_{ad}, the density of water, ρ_w, the height, h, the profile of radar reflectivity, $Z(h)$, and the profile of the subadiabatic function, $f(h)$. This approach for obtaining CDNC is also implemented in the SYRSOC algorithm. Determination of CDNC from the extinction coefficient with SYRSOC, as introduced by *Martucci and O'Dowd* [2011], works well for certain cloud cases. However, this retrieval is sensitive to uncertainties in the extinction profile. Due to necessary assumptions in the inversion of the ceilometer data, the algorithm cannot provide sufficiently accurate profiles of the extinction coefficient in all cases. Use of a Raman lidar and directly measured extinction coefficient profiles, at least at cloud base, could improve the extinction-based CDNC retrieval of SYRSOC. From CDNC, r_{eff}, LWC, COT, and cloud albedo were calculated. Vertical and temporal resolutions of the output are 15 m and 10 s.

Retrieval of r_{eff} and LWC was described by *Martucci and O'Dowd* [2011]. COT was calculated from a so-called reconstructed extinction coefficient, σ_{re}, obtained from the CDNC:

$$\sigma_{re}(h) = C * \left(N(h)^{1/3}\right) * \left(f(h) * A_{\text{ad}} * \left(h - h_{\text{cb}}\right)\right)^{2/3}, \tag{2}$$

with h_{cb} the cloud base altitude and

$$C = \pi^{1/3} * Q * k_2 * (4/3)^{-2/3} * \left(\rho_w/\rho_{\text{air}}\right)^{-2/3} * 10^5, \tag{3}$$

with the extinction efficiency Q, which is approximately 2 for the considered wavelength [*Boers et al.*, 2000], and k_2 depending on the shape parameter of the droplet size distribution [*Brandau et al.*, 2010, equation (20)]. COT is then obtained by integrating over the reconstructed extinction coefficient:

$$\text{COT} = \int \sigma_{re}(h)\text{d}h. \tag{4}$$

Cloud albedo is calculated from COT using a fixed ratio found by *Lacis and Hansen* [1974]:

$$\text{Albedo} = \text{COT}/(\text{COT} + 7.7). \tag{5}$$

The data set analyzed here includes clouds observed from February 2009 to April 2015. From these 6 years of cloud observations, homogeneous parts of less than 1 h duration of all single-layer nonprecipitating water clouds were selected. Maximum duration of 1 h was chosen to ensure homogeneity. Clouds were classified as homogeneous if cloud base and cloud top height changed by less than 50 m during that period and the variability in radar reflectivity was less than 1 dBZ. Selection of single-layer clouds was necessary because column LWP was used to calculate LWC profiles. Additionally, cases were restricted to nonprecipitating water clouds to match the monomodal droplet size distribution assumption of SYRSOC.

Large drizzle drops can have a strong impact on radar reflectivity without strongly affecting LWC [*Sauvageot and Omar*, 1987; *Fox and Illingworth*, 1997]. This distorts the calculation of microphysical cloud properties. As SYRSOC assumes monomodal size distributions, the drizzle mode cannot be represented. Drizzle was avoided by excluding regions of high radar reflectivity. In accordance with *Comstock et al.* [2004] and *Zuidema et al.* [2005], the threshold reflectivity for light drizzle was set to −17 dBZ.

The true uncertainties of the SYRSOC results are difficult to evaluate, because some contributions to the overall uncertainty can cancel each other. An uncertainty propagation approach would therefore lead to unrealistic results. Instead, a Monte Carlo approach was used to estimate uncertainties. Input parameters were randomly varied within the limits given in Table 1. Owing to the complexity of the calculations, this leads to 8000 samples per profile (i.e., per time step). The uncertainty was then calculated as the ratio of the standard deviation of the mean and the mean value of those 8000 samples. This can give an indication of the uncertainties introduced

Table 1. Input Parameters, Their Variability, and Number of Random Samples for Monte Carlo Error Estimation

Parameter	Instrument	Variability	Samples
Temperature	MWR	± 2 K	20
Liquid water path	MWR	± 20 g/m^2	20
Reflectivity	cloud radar	± 1 dBZ	20

by random errors in the measurements. Drizzle screening causes an additional bias for some cloud cases. This bias was estimated by running SYRSOC for clouds that included drizzle and for the same clouds with drizzle threshold applied. In drizzle-screened clouds, CDNC was on average about 60% higher and r_{eff} and LWC about 50% and 25% lower, respectively. There are further uncertainties related to drizzle, as both calculations for this estimate are based on the monomodality assumption. However, all SYRSOC results are obtained under a set of assumptions, mentioned earlier, which might not reflect reality and therefore could introduce further uncertainties, which are not discussed here. Uncertainties given with SYRSOC results below are those estimated by the Monte Carlo approach.

Three-day back trajectories from the National Oceanic and Atmospheric Administration (NOAA) HYSPLIT model (HYbrid Single-Particle Lagrangian Integrated Trajectory, *Draxler and Rolph* [2014]), were calculated for each case. Based on the prevailing synoptic situation and back trajectories, the cloud cases were classified as marine, coming from the Atlantic Ocean, or continental, coming from Europe. The classes “marine modified” and “continental modified” were introduced to categorize ambiguous cases: from the Atlantic, but with brief transport over Ireland or Great Britain, and for cases from Europe with transport over the ocean, respectively. Furthermore, black carbon (BC) concentrations measured in situ near the surface by a multiangle absorption photometer were used as further indication for clean cases. Marine cases with BC concentrations < 15 ng/m^3 were classified as clean marine, whereas all other marine cases were allocated to the marine modified class since they were likely influenced by anthropogenic sources [*O'Dowd et al.*, 2014; *Ovadnevaite et al.*, 2014]. Aerosol composition from the ground-based in situ aerosol mass spectrometer (AMS) [*Ovadnevaite et al.*, 2014] measurements were studied as well. AMS at Mace Head continuously samples SO_4, NH_4, NO_3, sea-salt, and organic aerosol concentrations. Fine-mode particulate matter (PM1) was obtained as sum of individual concentrations measured by the AMS. CCN concentrations near the surface were monitored with a Droplet Measurements Technology CCN counter [*Lance et al.*, 2006] at 0.75% supersaturation.

MODIS (Moderate-Resolution Imaging Spectroradiometer) level 2 data from both Terra and Aqua satellites [*Platnick et al.*, 2015a, 2015b] were used to verify the performance of SYRSOC. MODIS data at 3.7 µm, available at 1 km horizontal resolution, was only processed in cases of single-layered clouds. Data pixels with a cloud optical thickness smaller than 5 were removed, as the instrument might detect surface reflectance through these clouds. This would lead to unreliable retrieved cloud parameters for optically thin clouds.

3. Results

A total of 118 water clouds were analyzed for a better understanding of cloud microphysics as well as to provide insight into the impact of aerosols. Considering a data set of 6 years, this may seem like a small number, roughly covering 52 h of observations, especially since cloud-free conditions are rare at Mace Head. Instrument downtime was 20 to 25% per instrument (radar, ceilometer, and MWR), and they were seldom coincidental. Additionally, rigorous cloud screening limited the data set to the cases presented here. Using 3 day back trajectories, 78 of these cases were classified as marine (23 clean marine and 55 marine modified) and 40 cases were classified as continental (26 continental and 14 continental modified). Predominance of marine air masses reflects the overall Mace Head characteristics [*Jennings et al.*, 2003; *Reade et al.*, 2006], although *Jennings et al.* [2003] found only 52% of maritime air. This difference can be explained by the exclusive study of stratiform clouds within this work. The formation of stratiform clouds at Mace Head has a prevailing marine origin, while air masses from Europe are generally drier, thus suppressing cloud formation.

The 118 selected cloud periods were each about 10 to 30 min long. With a temporal resolution of 10 s they provided over 18,000 time steps. In total, 2339 of them were classified as clean marine, 9836 as marine modified, 4169 as continental, and 2516 as continental modified.

Table 2 contains information on the distribution of different air masses during the four seasons. Spring (March to May), autumn (September to November) and winter (December to February) were similar, with the

Table 2. Number of Time Steps Per Season and Their Fraction According to Air Mass Transport[a]

	MAM	JJA	SON	DJF
Total number	3927	6235	4411	4287
Fraction marine	9%	22%	6%	8%
Fraction marine modified	37%	75%	44%	41%
Fraction continental modified	23%	3%	16%	17%
Fraction continental	31%	0%	34%	34%

[a]MAM (March–May) = spring; JJA (July–August) = summer; SON (September–November) = autumn; and DJF (December–February) = winter.

most cloud cases in marine modified conditions, followed by continental, continental modified, and marine. Conditions were very different for clouds observed in summer (June to August). Stratiform clouds were almost exclusively observed during marine and marine modified periods. Only a few cloud cases were recorded for continental modified air masses.

3.1. Air Mass Characterization

Figure 1 shows the distributions of BC, CCN, and PM1 concentrations at ground level during the cloud observations. In situ data were not available for all cloud cases. The number of data points in each distribution is shown on the top axis. Figure 1d also shows SYRSOC CDNC concentrations for comparison. SYRSOC results are discussed in section 3.2.2 below. Generally, BC concentrations agreed well with the trajectory analysis, showing higher concentrations for air masses advected from the continent and lower concentrations for air masses transported over the Atlantic (Figure 1a). This is reflected in all mean values and percentiles shown. The medians (and mean values) were 5 ng/m^3 (5 ng/m^3) for marine cases, 24 ng/m^3 (33 ng/m^3) for marine modified cases, 60 ng/m^3 (89 ng/m^3) for continental modified cases, and 127 ng/m^3 (230 ng/m^3) for continental cases. The overall spread is largest for the continental class, ranging from 41 ng/m^3 to 774 ng/m^3 (5th and 95th percentiles).

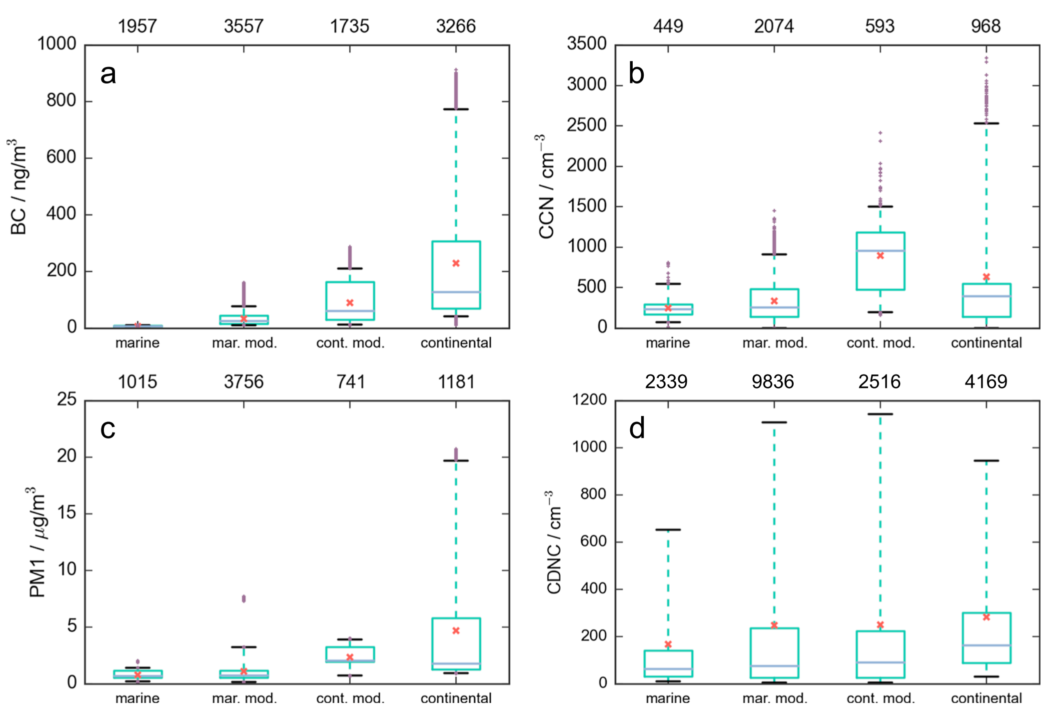

Figure 1. Box plots of (a) BC, (b) CCN, (c) PM1, and (d) CDNC concentrations, sorted by the air mass transport according to HYSPLIT back trajectories (mar. mod. = marine modified; cont. mod. = continental modified). Shown are the median (blue horizontal line), 25th and 75th percentiles (box), 5th and 95th percentiles (whiskers), mean value (red cross), and data points out of the 5th to 95th percentiles (purple dots). The number of data points per class is shown on the top axis.

The lowest CCN mean value was found for marine cases with 230 cm^{-3}, while the median was 250 cm^{-3}. Both, median and mean CCN concentrations, marine modified cases were slightly larger than those of marine cases with 260 cm^{-3} and 340 cm^{-3}, respectively. CCN concentrations of continental modified cases were on average highest (Figure 1b) with median and mean of 960 cm^{-3} and 890 cm^{-3}, respectively. The highest absolute values were observed in continental air masses. However, this 400 cm^{-3} median was closer to marine and marine-modified medians. This indicates no clear relationship between CCN concentrations and air mass transport paths. This is due to the fact that not only BC but also other components like SO_4 and sea salt can act as CCN [*Pierce and Adams*, 2006; *O'Dowd et al.*, 1999].

Mean PM1 concentrations and overall distributions well represented the air masses (Figure 1c). During 95% of marine cases, PM1 was below 1.4 μg/m^3, median and mean value were 0.68 μg/m^3 and 0.76 μg/m^3, respectively. All shown percentiles were similar or higher for marine modified cases, and all were even higher for continental modified cases. The medians (and mean values) for those two classes were 0.74 μg/m^3 (1.12 μg/m^3) and 2.04 μg/m^3 (2.37 μg/m^3), respectively. Highest PM1 concentrations were observed within continental air masses, where 95th percentile, 75th percentile, 5th percentile, and mean (4.70 μg/m^3) were highest. The 1.79 μg/m^3 median and 25th percentile (1.25 μg/m^3) were lower than median and 25th percentile of the continental modified class.

BC, CCN, and PM1 concentrations in Figure 1 show a smaller spread between the 25th and 75th percentiles of the marine and marine modified cases than those of the continental modified and continental cases. Relative broadness with respect to mean was also smaller in marine cases than in continental cases. This is especially remarkable, because the marine modified class includes the largest number of data points. This hints at more uniform conditions at ground level during air mass advection from the Atlantic. Air masses from Europe can contain different grades of pollution and mixtures of different aerosol types. Additionally, the ground-based in situ observations in these cases were more likely influenced by local and regional emissions.

Box plots for BC and PM1 per season are shown in Figure 2. Median, 25th percentile, and 75th percentile of seasonal BC, CCN, and PM1 concentration distributions are also listed in Table 6. Distributions of BC and PM1 concentrations were very narrow in summer with 25th percentile and 75th percentile of 7 ng/m^3 and 34 ng/m^3 (BC) and 0.64 μg/m^3 and 1.21 μg/m^3 (PM1). Median and mean were 15 ng/m^3 and 24 ng/m^3 (BC) and 0.86 μg/m^3 and 1.28 μg/m^3 (PM1). All spring percentiles were higher with median, 25th percentile, and 75th percentile of 39, 14, and 67 ng/m^3 (BC) and 0.88, 0.71, and 1.86 μg/m^3 (PM1). Narrow distributions during spring and summer were observed for SO_4, NH_4, NO_3, and organic aerosol concentrations (not shown). The BC autumn distribution was widest with median, 25th percentile, and 75th percentile of 61, 18, and 206 ng/m^3. In winter, median was largest with 106 ng/m^3. Few cases of very high BC concentrations (shown as outliers) were detected in spring, autumn, and winter. The highest BC concentrations were observed in autumn. PM1 distributions were broader in spring and winter, compared to summer and autumn (Figure 2b), with much higher 95th percentile. Highest PM1 concentrations were detected in spring. Relative broadness with respect to mean was largest in autumn. Median CCN concentrations (Table 6) were similar in spring and summer. Highest mean values, percentiles, and extreme values of CCN were observed in winter, which might indicate an influence of local pollution due to household heating. Enhanced sea-salt concentrations due to high wind speeds, which occur more frequently in winter [*Mulcahy et al.*, 2008; *Yoon et al.*, 2007], likely contributed to the CCN concentrations. On average, CCN concentrations were lowest in autumn.

3.2. Ground-Based Remote Sensing

One advantage of active remote sensing methods such as radar and lidar is the possibility to observe vertical distributions of scatterers at high range resolution. In the following, the observed cloud base and top heights as well as the cloud depth are discussed. Cloud base altitude was obtained from ceilometer data and cloud top altitude from radar reflectivity, by analyzing signal gradients [*Martucci et al.*, 2010].

3.2.1. Cloud Boundaries

As mentioned above, only homogeneous single-layer nonprecipitating water clouds were included in this study. They barely reached cloud top altitudes greater than 2.5 km above ground level (agl). Most of the clouds were 260 to 420 m deep. The medians and percentiles (25% and 75%) of the cloud boundaries and cloud depths are shown in Table 3. The seasonal behavior of the cloud base altitudes was similar to the cloud top altitudes. Cloud base medians were highest in summer and lowest in spring. Cloud top median were highest in summer and autumn and lowest in spring. Cloud depths were slightly larger in autumn and winter with

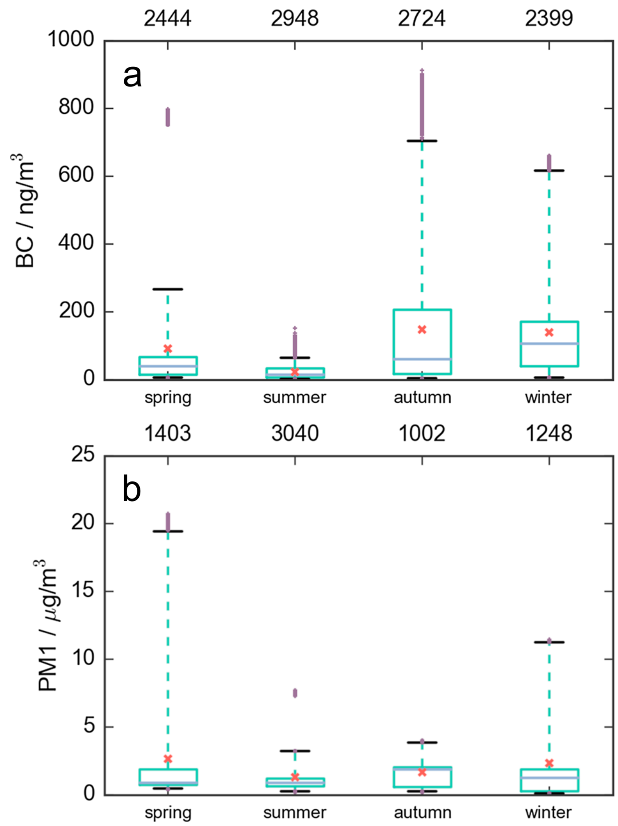

Figure 2. Box plots of (a) BC and (b) PM1 concentrations, sorted by season (spring = March to May, summer = June to August, autumn = September to November, and winter = December to January). Shown are the median (blue horizontal line), 25th and 75 percentiles (box), 5th and 95th percentiles (whiskers), mean value (red cross), and data points out of the 5th to 95th percentiles (purple dots). The number of data points per class is shown above the top axes.

medians of 0.34 and 0.35 km, respectively, suggesting a larger water vapor vertical flux during these seasons. Medians during spring and summer were 0.33 and 0.32 km, respectively.

Figure 3 shows hour average cloud base heights (Figure 3a) and cloud depths (Figure 3b) for all clouds. Local time is the same as UTC in winter and UTC+1 h in summer. Each hourly interval includes 140 to 1510 data points. No clear diurnal cycle is indicated. The spread of cloud base values (5th and 95th percentiles) was larger during nighttime and morning, whereas the 25th and 75th percentiles included a larger range during the day. The hourly distributions of cloud depths were stable throughout the day, with slightly increased ranges in late afternoon and evening. Such small diurnal variation in cloud depth can be expected for the studied stratiform cloud type.

Cloud boundary dependence on air masses are given in Table 4. Again, cloud base and cloud top heights showed a similar pattern. On average, clouds observed during marine air mass advection were slightly higher and thinner than those in continental cases. The small variation may be explained by the focus of this study on one particular cloud type. Selection of drizzle-free clouds limits the data set to shallow clouds, because thicker clouds will inevitably form drizzle. Moreover, limitation to liquid clouds restricts cloud base and top altitudes.

Table 3. Median and Range (25%–75%) of Cloud Top Altitude, Cloud Base Altitude, and Cloud Depth by Season

	Spring (MAM)	Summer (JJA)	Autumn (SON)	Winter (DJF)
cloud top (km agl)	1.0 (0.9–1.4)	1.4 (1.1–1.6)	1.4 (1.2–1.5)	1.1 (1.0–1.3)
cloud base (km agl)	0.7 (0.5–1.1)	1.1 (0.6–1.3)	1.0 (0.8–1.3)	0.8 (0.6–1.0)
cloud depth (km)	0.33 (0.26–0.42)	0.32 (0.27–0.39)	0.34 (0.27–0.41)	0.35 (0.30–0.42)

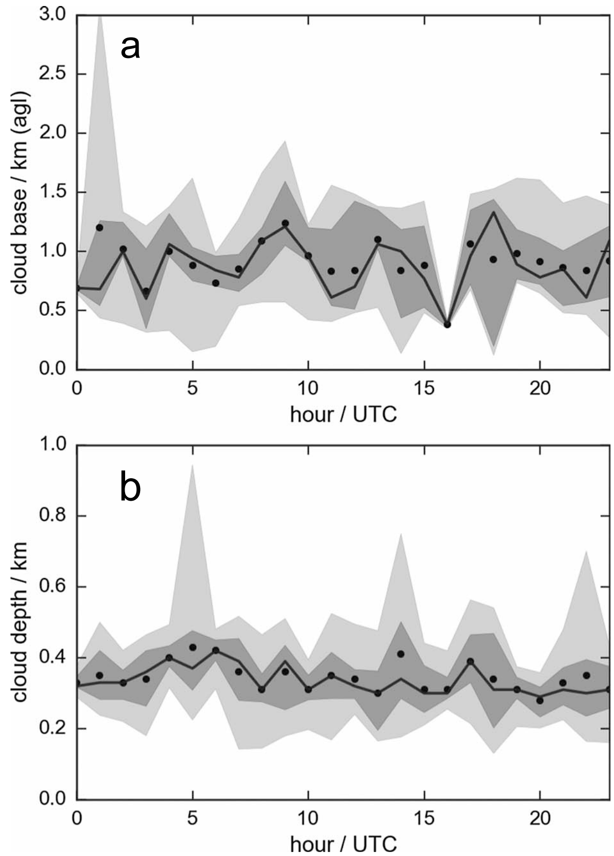

Figure 3. Daily cycle of (a) cloud base altitude and (b) cloud depth. Shown are the median (black line), 25th and 75th percentiles (dark gray shaded area), 5th and 95th percentiles (light gray shaded area), and mean values (dots).

3.2.2. Microphysical Cloud Properties

CDNC, r_{eff}, and LWC were averaged over the duration of the individual cloud periods between about 10 and 30 min. The mean in-cloud profiles were then normalized to cloud depth, so that each profile starts at 0 and ends at 1. Figure 4 shows profiles of a marine example case of 28 July 2010 and a continental case of 2 September 2014. The marine CDNC profile from 28 July 2010 was fairly constant with height. This agrees with the marine clouds of *Miles et al.* [2000] and *Noble and Hudson* [2015]. CDNC on 2 September 2014 (continental case) increased at cloud base and top. CDNC increase at the cloud top may indicate entrainment from above. Mixing of CCN into the cloud would increase CDNC and reduce r_{eff}. Another explanation might be nonuniform radar beam filling at the cloud boundaries, which leads to a virtual decrease in reflectivity in the first or last range bin, also resulting in smaller r_{eff} and larger CDNC. *Miles et al.* [2000] found large variations in profile shapes of CDNC in continental clouds.

Median r_{eff} generally increased from cloud base to cloud top, with a slight decrease near the top on 2 September 2014, corresponding to the CDNC increase. LWC followed a subadiabatic profile with a subadiabaticity of about 0.18 on 28 July 2010 and 0.07 on 2 September 2014. Increasing LWC from cloud base

Table 4. Number of Time Steps As Well As Median and Range (25%–75%) of Cloud Top and Base Altitude and Cloud Depth by Air Mass Transport

	Marine	Marine Modified	Continental Modified	Continental
Total number	2339	9836	2516	4169
Cloud top (km agl)	1.2 (0.9–1.4)	1.4 (1.1–1.5)	1.1 (0.9–1.3)	1.3 (1.0–1.5)
Cloud base (km agl)	0.8 (0.5–1.1)	1.0 (0.7–1.2)	0.7 (0.4–0.8)	0.9 (0.6–1.2)
Cloud depth (km)	0.31 (0.23–0.44)	0.33 (0.27–0.39)	0.37 (0.31–0.44)	0.35 (0.28–0.42)

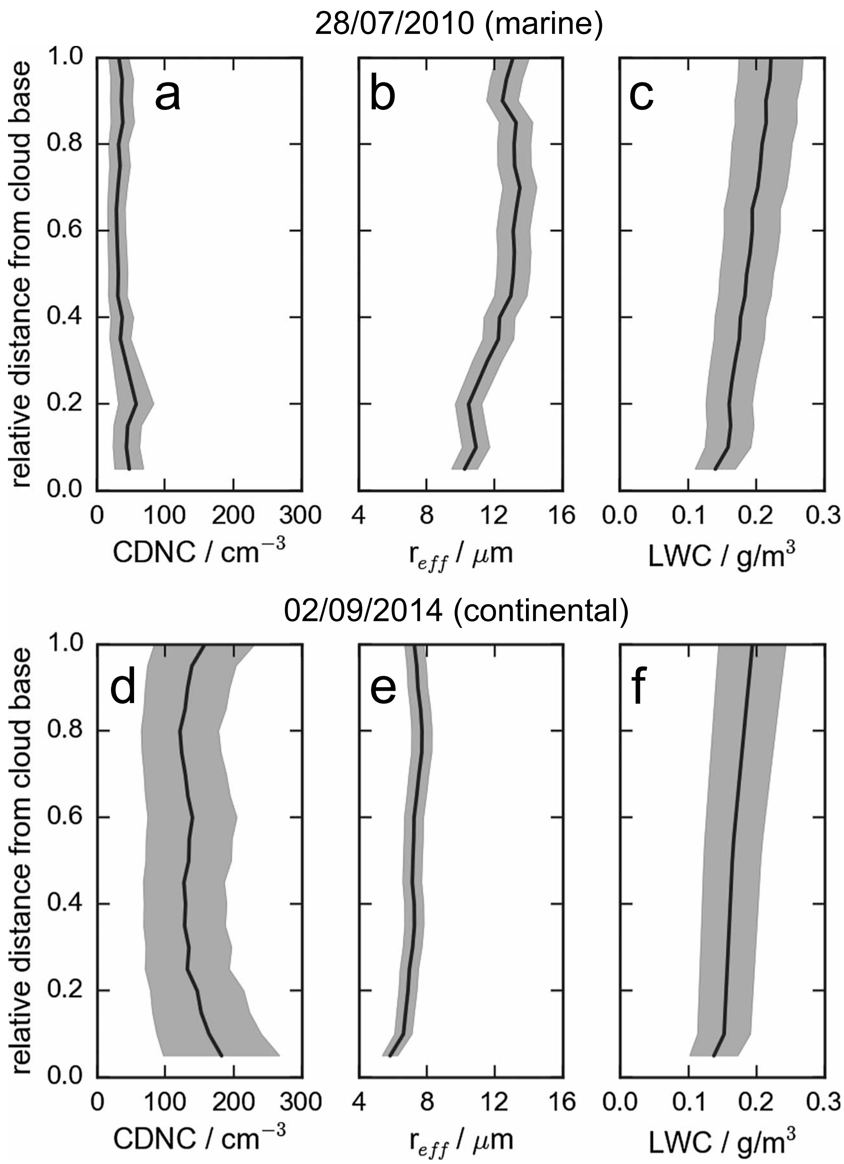

Figure 4. Profiles of (a, d) CDNC, (b, e) r_{eff}, and (c, f) LWC on 28 July 2010 (Figures 4a–4c) and 2 September 2014 (Figures 4d–4f). Shown are median (black line) and uncertainties obtained by Monte Carlo approach (shaded area).

throughout the cloud was also found by *Miles et al.* [2000], *Hudson and Yum* [1997], and *Noble and Hudson* [2015]. Uncertainties in the marine (and continental) case were about 43% (45%), 7% (8%), and 21% (24%) for CDNC, r_{eff}, and LWC, respectively.

Relative uncertainties (err), obtained by the Monte Carlo approach, were averaged over all profiles. They were nearly constant with altitude, only slightly higher at cloud base, for all three microphysical cloud properties (not shown). Median err_{CDNC} was below 50%. The 25th and 75th percentiles of err_{CDNC} were 30% and 80%. The 25th and 75th percentiles of err_{LWC} spread from about 10% to 40%, with a median of 20%. Median and range of $err_{r_{eff}}$ were lowest, ranging between 5 and 15%.

Results discussed in the following, contain data of the entire cloud, except those parts excluded by the radar reflectivity threshold. The normalized distributions of CDNC, r_{eff}, and LWC are plotted in Figure 5 according to the air mass transports. The corresponding medians and 25th and 75th percentiles are given in Table 5.

Medians and percentiles of CDNC were smallest for clean marine air masses (see also Figure 1d). The distribution of marine cases was monomodal, whereas the marine modified cases showed a slightly bimodal behavior, with broad modes centered near 60 and 150 cm^{-3} (Figure 5a). This indicates a mixture of air masses but might

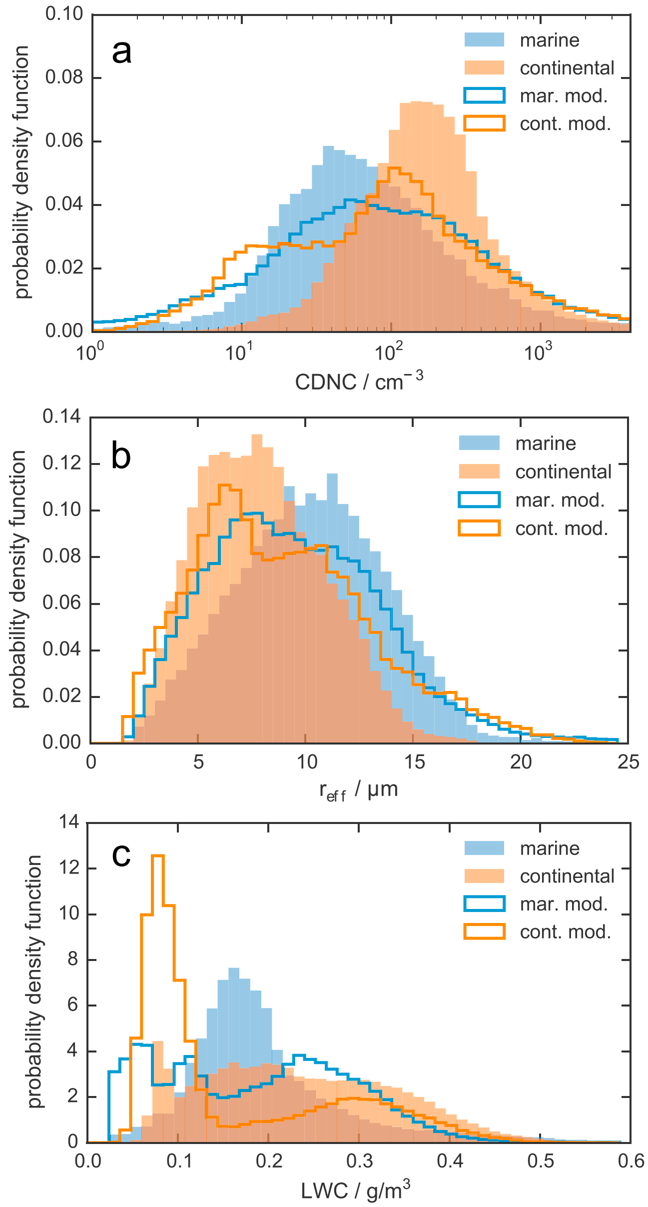

Figure 5. Distributions of (a) CDNC (logarithmic scale), (b) r_{eff}, and (c) LWC by air mass transport. Modified air masses (mar. mod. = marine modified; cont. mod. = continental modified) are plotted as lines.

also be due to air mass misclassification based on back trajectories. The bimodal continental modified CDNC distributions had one broad mode centered near 20 cm^{-3} and one peak near 100 cm^{-3}. Relative to the other air mass classes, few cloud cases were classified as clean marine or continental modified. This means that one outlier can strongly influence these distributions, which would produce broader or multiple modes. The distribution of continental cases had one peak near 200 cm^{-3}. On average, the CDNC was highest for continental cases, although small fractions of high CDNC were also found in the modified air mass types.

The marine r_{eff} distribution was wider than in continental conditions (Figure 5b). The median r_{eff} was 10 μm and 9 μm for marine and marine modified air masses. The r_{eff} distribution of marine modified cases was bimodal with the main peak near 8 μm and one at 12 μm. As with the CDNC distribution, this indicates the influence of both clean and polluted air masses within this class. Continental modified cases also showed a bimodal distribution for the same reasons, as mentioned before. The main peak was near 7 μm, and the smaller one was near 11 μm. The distribution of r_{eff} in continental cases had a broad mode centered at 7 μm.

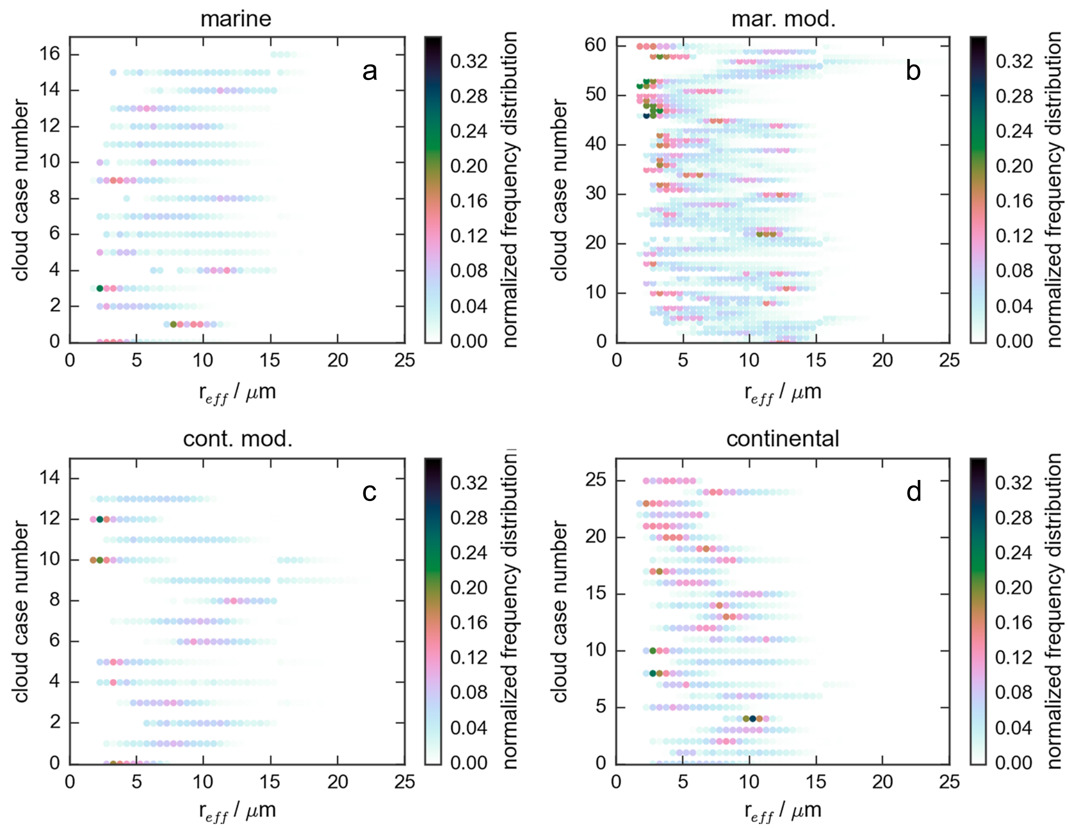

Figure 6. Size distributions, color coded according to the normalized frequency distribution, separately for each cloud case. Each panel shows a different air mass (mar. mod. = marine modified; cont. mod. = continental modified).

These results confirm the inverse relationship between CDNC and r_{eff} in agreement with the literature [*Ferek et al.*, 2000; *Lohmann and Feichter*, 2005]. This relationship is forced by the algorithm at each time step. However, the data set studied here confirms the general validity of this assumption from more than 18,000 time steps. All distributions of CDNC and r_{eff} were broad, covering a wide range of values. This is due to the large number of data points and the coarse estimation of the air mass transport path 3 days prior to observation. Investigation of the actual origin of air masses and aerosol content at cloud level was not part of this study. Classification uncertainties would produce broader distributions. Averaging over whole cloud profiles contributes to further broadening. However, the peaks and medians can be considered statistically robust, owing to the number of time steps.

LWC distributions (Figure 5c) show two or more peaks for all classes except clean marine, which has one peak near 0.17 g/m^3. Whereas the medians were similar for marine, marine-modified, and continental cases, the median of continental modified cases was much lower due to a strong peak just below 0.1 g/m^3. The distribution of marine modified conditions had not only small peaks near 0.05 g/m^3 and 0.12 g/m^3 but also a broader mode centered near 0.23 g/m^3. The peak of the marine modified LWC distribution at 0.05 g/m^3 was linked to small LWP (10–20 g/m^2). LWC distributions for continental cases also had several modes, with a narrow one at 0.08 g/m^3 and two broad ones centered at 0.2 g/m^3 and 0.3 g/m^3. Median, 25th and 75th percentiles of continental LWC distributions were the highest. This seems counterintuitive; however, drizzle was excluded from this data. The more polluted air masses advected from the continent probably held more liquid water before forming drizzle than the cleaner air masses from the ocean. This would be due to rain suppression in more polluted air masses [*Albrecht*, 1989; *Hudson and Yum*, 2001; *Yum and Hudson*, 2002; *Hudson et al.*, 2009], i.e., second indirect aerosol effect [*Hudson*, 1993]. Moreover, some nondrizzling cloud parts with small CDNC, high r_{eff}, and high LWC possibly were removed from this analysis by applying the reflectivity threshold.

Individual droplet size distributions were calculated separately for each cloud case from r_{eff} and CDNC. The averaged distributions normalized by CDNC are shown in Figure 6. Each horizontal line represents the cloud droplet size distribution of one cloud case, with darker colors at high normalized frequencies and lighter colors

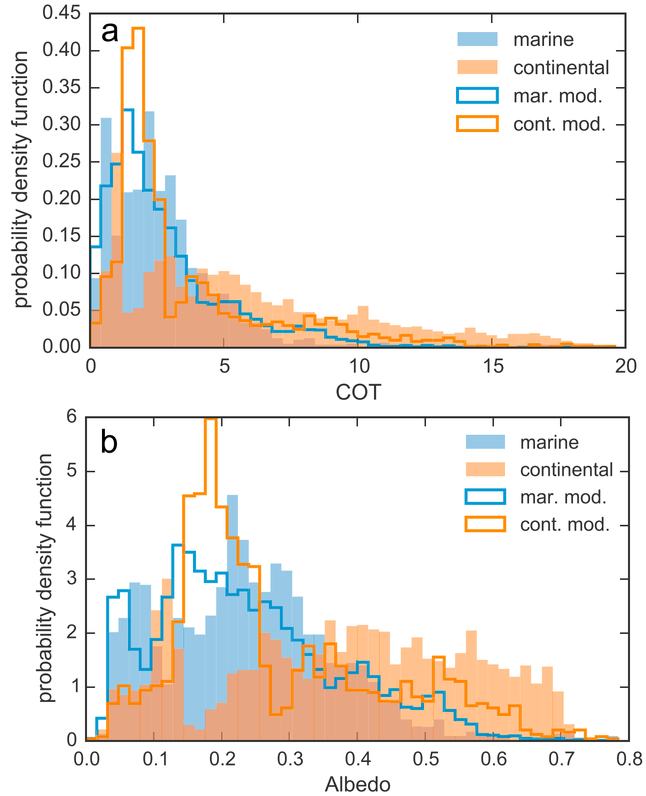

Figure 7. Distributions of (a) COT and (b) cloud albedo by air mass transport. Modified air masses (mar. mod. = marine modified; cont. mod. = continental modified) are plotted as lines.

at low normalized frequencies. Overall, the marine and marine-modified size distributions (Figures 6a and 6b) were broader, with lower maxima, than the continental size distributions (Figure 6d), which showed more pronounced peaks at smaller r_{eff}. Already in the 1950s, *Squires* [1958] found broad distributions associated with low CDNC and *Hudson and Yum* [1997] confirmed that the size distribution broadening in marine stratus is associated with larger r_{eff}. Very high maxima at low r_{eff} in some marine and marine-modified cases might indicate problems with drizzle detection or long-range transport of aerosol at cloud altitude.

Cloud optical properties were also investigated. Figure 7 shows distributions of COT and cloud albedo. COT median, 25th percentile and 75th percentiles were similar for marine, marine-modified, and continental-modified cases (Table 5). The main peaks of these distributions were at 2.5, 2.1, and 2.3, respectively. The two modified classes show a second broad mode centered near 5 (marine modified) and 4 (continental modified). The distribution of the continental cases looks very different. There is one sharp peak at COT of 1, a smaller peak near 3 and a broad mode centered near 5. The percentiles reflect this difference. Median, 25th percentile, and 75th percentiles were highest for continental cases.

Table 5. Median and Range (25%–75%) of Cloud Properties by Air Mass Transport

	Marine	Marine Modified	Continental Modified	Continental
CDNC (cm^{-3})	60 (30–140)	80 (30–230)	90 (20–220)	160 (90–300)
r_{eff} (μm)	10 (8–13)	9 (7–12)	9 (6–12)	8 (6–10)
LWC (g/m^3)	0.18 (0.14–0.23)	0.19 (0.10–0.27)	0.10 (0.08–0.26)	0.22 (0.15–0.31)
LWP (g/m^2)	70 (37–94)	70 (36–103)	36 (26–111)	75 (44–131)
f	0.10 (0.09–0.14)	0.12 (0.06–0.16)	0.09 (0.06–0.17)	0.15 (0.09–0.23)
COT	2.4 (1.3–3.6)	2.1 (1.2–3.6)	2.2 (1.6–4.7)	4.9 (2.5–8.7)
Albedo	0.23 (0.15–0.32)	0.22 (0.14–0.32)	0.23 (0.17–0.38)	0.39 (0.24–0.53)

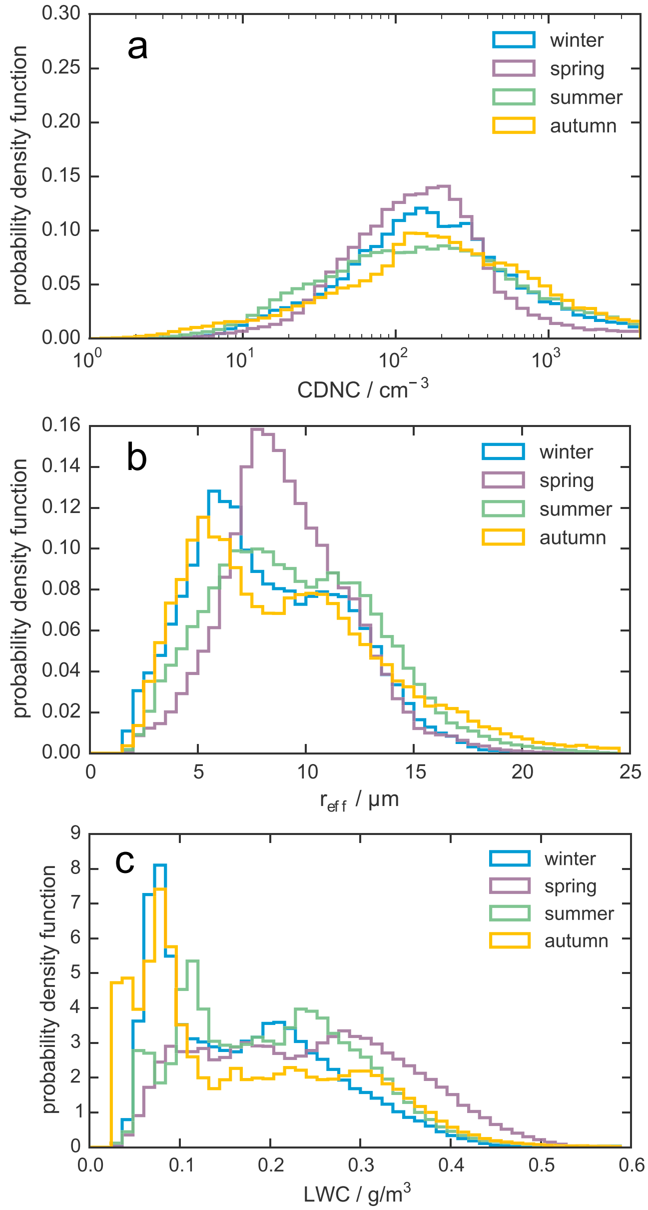

Figure 8. Distributions of (a) CDNC, (b) r_{eff}, and (c) LWC by season.

Similar to COT, there were clear cloud albedo differences between marine and modified classes and the continental class. Median, 25th percentile, and 75th percentiles of the two marine distributions and the continental-modified distribution were similar, with the smallest median and 25th percentile for marine-modified cases but smallest 75th percentiles for marine cases. The cloud albedo distributions in Figure 7b show two main peaks of the marine distribution at 0.08 and 0.22. Those first peaks of marine and marine modified cases are likely related to small LWP. There is another broad peak of the marine modified distribution at 0.14 followed by small broad modes centered near 0.41 and 0.52. The continental modified distribution has one sharp peak at 0.2, followed by some smaller broad modes at higher values. Moreover, there is a very broad main distribution for continental cases with albedos higher than 0.2 and an additional narrow peak centered at 0.12. Mean values of albedo and COT were lower in marine and marine-modified air than in continental and continental-modified air.

Overall, COT and albedo were lower in cleaner air masses and higher in more polluted conditions, which is in agreement with *Twomey* [1977], *Brenguier et al.* [2003], and others. Lower COT and albedo medians were linked to high r_{eff} medians and low CDNC medians for marine and marine-modified cases (Table 5), and vice versa

Table 6. Median and Range (25%–75%) of Cloud Properties, As Well As BC, CCN, and PM1 Concentrations by Season

	Spring (MAM)	Summer (JJA)	Autumn (SON)	Winter (DJF)
CDNC (cm^{-3})	110 (50–220)	80 (30–250)	100 (20–280)	110 (40–260)
r_{eff} (μm)	9 (7–11)	9 (7–12)	8 (5–11)	9 (6–12)
LWC (g/m^3)	0.24 (0.15–0.32)	0.20 (0.12–0.27)	0.14 (0.08–0.26)	0.16 (0.09–0.24)
LWP (g/m^2)	75 (35–134)	69 (37–102)	51 (22–100)	76 (38–104)
f	0.17 (0.10–0.24)	0.11 (0.07–0.14)	0.09 (0.03–0.14)	0.14 (0.09–0.19)
COT	3.7 (1.7–8.0)	2.3 (1.4–3.6)	1.8 (1.1–3.8)	2.8 (2.0–5.0)
Albedo	0.32 (0.18–0.51)	0.23 (0.15–0.31)	0.19 (0.13–0.33)	0.27 (0.21–0.39)
BC (ng/m^3)	39 (14–67)	15 (7–34)	61 (18–206)	106 (40–172)
CCN (cm^{-3})	440 (200–760)	370 (230–500)	180 (70–400)	520 (240–1250)
PM1 ($\mu g/m^3$)	0.9 (0.7–1.9)	0.9 (0.6–1.2)	1.9 (0.6–2.0)	1.3 (0.2–1.9)

for continental cases. The seemingly contradictory behavior in continental modified cases can be attributed to a strong peak at low LWC (Figure 5c). A similar LWC peak, although lower, is present in marine modified cases and might be linked to transport paths influenced by both, marine and continental conditions. Table 5 also shows minimum LWP and, consequently, lowest median subadiabaticity in continental modified cases. This did not impact CDNC or r_{eff} but strongly influenced the calculation of COT and albedo.

Besides air mass classification, a separate analysis of the distributions of microphysical cloud properties by season was done. CDNC, r_{eff} and LWC are shown in Figure 8. The medians, 25th percentile, and 75th percentile of these distributions are also listed in Table 6. The shapes of all CDNC distributions were similar, as were the medians, 25th percentile and 75th percentiles in spring, autumn, and winter with lower values in summer. This indicates stronger influence of continental air masses during these seasons compared to summer. Indeed, Table 2 gives the highest proportion of continental plus continental modified cases in spring, with 54%, followed by winter (51%) and autumn (50%). Median CDNC was lowest in summer (Table 6). This can be explained by the observed air mass characteristics. No continental and very few continental modified cases were observed in summer (Table 2), most likely because the continental air masses transported from Europe were characterized by thermodynamic conditions less favorable to the formation of the stratiform clouds investigated in this study, e.g., higher mean temperature, lower relative humidity, and larger convective available potential energy. Of the 6235 summer data points, 22% were marine and 75% were marine modified (Table 2). BC and PM1 concentrations were also smallest during summer (Table 6), which thus agreed with the observed air mass types.

Differences in r_{eff} were less pronounced in medians, 25th percentile and 75th percentile (Table 5) than in distribution shapes. The only monomodal distribution, though broad, was obtained from spring cases. This may be due to the smaller number of data points, relative to the other seasons (see Table 2). The median and 25th percentile of r_{eff} in autumn were slightly lower than those during the other seasons. Median LWC was lowest in autumn and highest in spring. As mentioned earlier, this is linked to the high LWP and consequently less adiabatic conditions in autumn. Seasonal values of LWP and subadiabaticity, f, are listed in Table 6. Unlike all other seasonal distributions, the spring distribution does not show a peak at low LWC. The optical properties by season are also given in Table 6. The link between LWC, subadiabaticity, and optical properties forced by the algorithm is clearly represented, with low COT and albedo at low LWC, and vice versa. COT and albedo medians were higher in winter and spring than in summer and autumn.

3.3. Comparison With MODIS

Out of the data set described above, 40 cases were coincident with overpasses of the Aqua or Terra satellite over Mace Head. These cases were used for a comparison of SYRSOC results with MODIS cloud products at 3.7 μm [*Platnick et al.*, 2015a, 2015b], namely, r_{eff} at cloud top, the cloud water path (CWP or LWP), and COT. MODIS data were averaged over an area from 53.27 to 53.37°N and from −9.91 to −9.89°E, with Mace Head at its center. MODIS pixels with COT smaller than 5 were removed before averaging. MODIS provided uncertainties of COT, LWP, and r_{eff} ranging from 3% to 15%, 10% to 28%, and 5% to 9%, respectively.

SYRSOC produces profiles of the microphysical cloud properties. However, MODIS has a very small penetration depth into clouds and therefore only retrieves microphysical cloud properties near cloud top. Therefore,

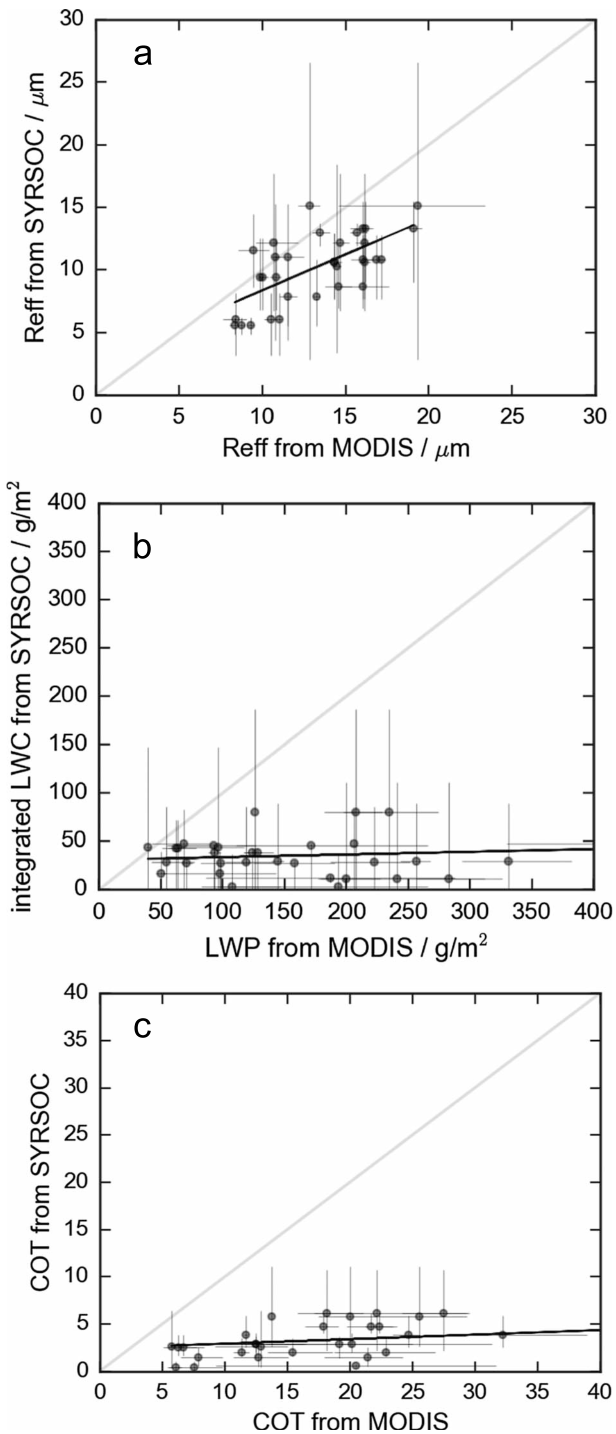

Figure 9. Comparison of (a) r_{eff}, (b) integrated LWC/LWP, and (c) COT from MODIS and SYRSOC. Dots mark mean values, and error bars span minima to maxima. The 1:1 line and linear fit are shown in gray and black, respectively.

SYRSOC r_{eff} was averaged from 75 to 45 m below the radar detected cloud top (three data points), while LWC was integrated over the full cloud depth. Subsequently, r_{eff}, COT and integrated LWC were averaged about 10 min before and 10 min after the overpass. The comparisons of mean values for all available cases are shown in Figure 9. Error bars represent minimum and maximum values. The best linear fits of MODIS products and SYRSOC results were calculated. Regression lines are plotted, and fitting parameters are given in Table 7.

Table 7. Fitting Parameters of the Linear Fit of MODIS Products and SYRSOC Results

	Slope		*y* Intercept		R [R^2]	
	With Drizzle	Without Drizzle	With Drizzle	Without Drizzle	With Drizzle	Without Drizzle
Effective radius	0.95	0.57	−1 μm	3 μm	0.67 [0.45]	0.65 [0.43]
Integrated LWC	0.11	0.03	50 g/m^2	31 g/m^2	0.38 [0.14]	0.20 [0.04]
LWP	0.11	0.11	57 g/m^2	57 g/m^2	0.36 [0.13]	0.36 [0.13]
COT	0.05	0.05	2	2	0.44 [0.19]	0.43 [0.18]

The r_{eff} seems to be systematically underestimated by SYRSOC or overestimated by MODIS. In most cases, SYRSOC r_{eff} showed a larger variability than MODIS r_{eff}. COT was also underestimated by SYRSOC or overestimated by MODIS to a greater extent at higher COT. MODIS COT ranges were larger than SYRSOC COT ranges. As mentioned earlier, drizzle detection is done by SYRSOC to assure stability of the algorithm and representable results. However, this screening process can exclude parts of the clouds that MODIS detects. This is obvious in the comparison of the integrated LWC with MODIS LWP. Cloud areas with high LWC are excluded, and therefore, the integrated values are lower than the MODIS LWP.

LWP was measured directly from ground by the MWR. These data were used as input for SYRSOC. For the 40 cloud cases, LWP from the ground-based radiometer at Mace Head was compared with MODIS LWP (Figure 10). The agreement of directly measured LWP was clearly better than the agreement of SYRSOC results with MODIS products. However, there were large differences, especially at high-mean LWP, where the variability of both instruments was larger. Measurement and retrieval uncertainties should be considered as well. They were estimated to be 20 g/m^2 for MWR LWP and were provided as 10% to 28% of MODIS LWP. Integrated SYRSOC LWC was in many cases lower than MWR LWP because of SYRSOC drizzle screening.

In order to test the assumption that LWP differences were due to drizzle screening, the SYRSOC run was repeated without drizzle screening. The resulting comparisons of SYRSOC and MODIS are shown in Figure 11. The mean and maximum SYRSOC r_{eff} was higher for cases affected by drizzle. The mean values of integrated LWC from SYRSOC agreed much better with the input LWP from the ground-based MWR in the drizzle run (compare Figure 10). In addition, agreement with satellite LWP was improved.

The fitting parameters for runs with and without drizzle screening are listed in Table 7. The correlations of r_{eff} and LWC were better for the run with drizzle. The agreement of LWP from the MWR changed because time steps were added that were not included earlier due to drizzle screening. The integrated LWC agreed better with the MODIS LWP with drizzle included. The correlation of COT was greater when drizzle was included. Apart from r_{eff} with a slope near 1 and small offset, overall agreement was poor. Comparison with MODIS products at 1.6 and 2.1 μm showed similar results. SYRSOC is based on the assumption of

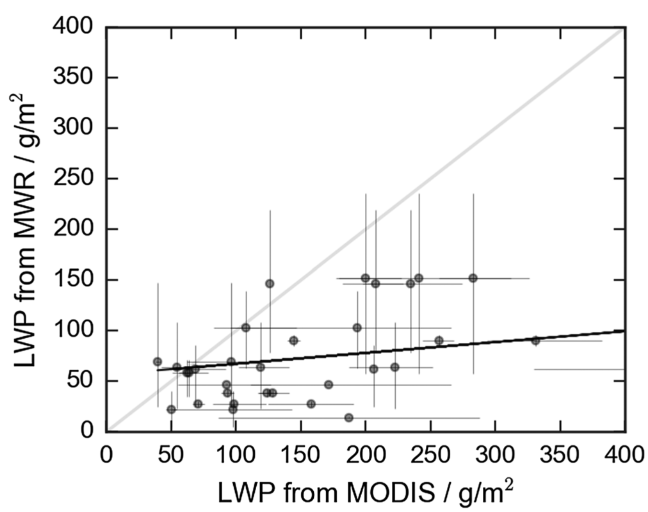

Figure 10. Comparison of MODIS LWP with LWP from the ground-based MWR. Dots mark mean values, and error bars span minima to maxima. The 1:1 line and linear fit are shown in gray and black, respectively.

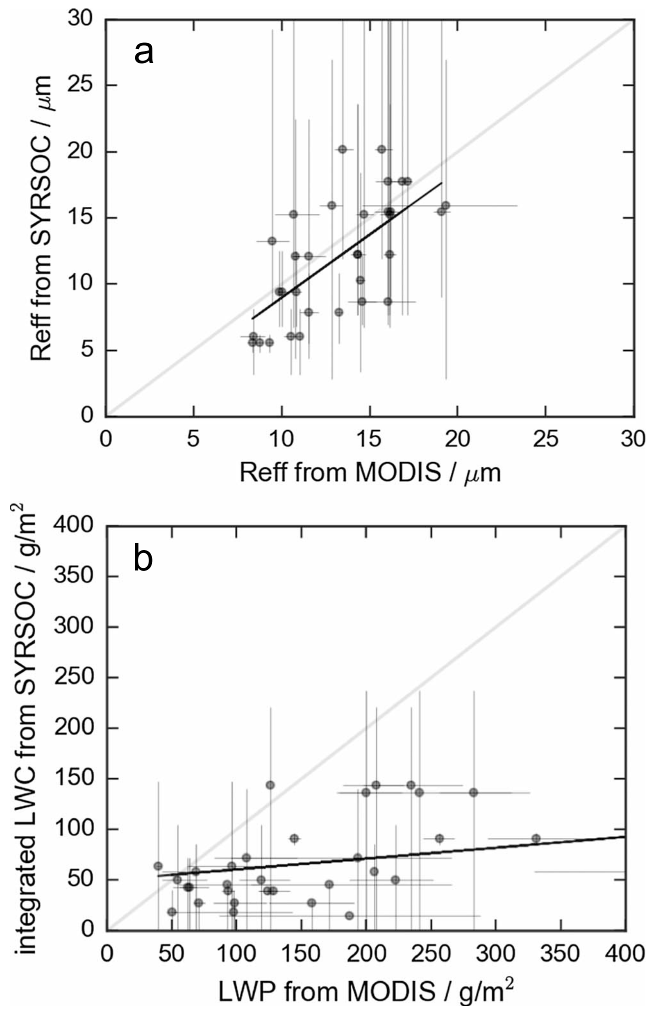

Figure 11. Comparison of (a) r_{eff} and (b) integrated LWC/LWP from MODIS and SYRSOC, including downdrafts and drizzle. Dots mark mean values, and error bars span minima to maxima. The 1:1 line and linear fit are shown in gray and black, respectively.

a monomodal gamma size distribution, which thus does not include drizzle. Therefore, even including time steps affected by drizzle, a realistic representation of drizzle properties cannot be provided. This limits a comparison of our carefully selected data with an all-cloud average from MODIS. This work focusses on temporal homogeneity over 10 min to a maximum of 1 h. This can include horizontally inhomogeneous clouds, especially since they are observed at a land-sea boundary. Surface inhomogeneity can affect cloud properties.

4. Conclusions

Ground-based remote sensing observations of cloud microphysical properties have been made at the coastal site of Mace Head, Ireland, starting in 2009. Homogeneous single-layer nonprecipitating water clouds were selected from a 6 year database. This comprehensive study of 118 cloud cases with a total of more than 18,000 data points (time steps) is statistically representative, compared to single case studies. It is, to the authors' knowledge, the first work analyzing a large number of stratiform liquid water clouds observed at a coastal site over a period of more than 6 years using a synergy of three ground-based remote sensing instruments. The size of the studied data set and the comprehensive air mass characterizations allow a robust interpretation of the results.

Ground-based in situ measurements of aerosol concentrations also revealed the cleanest conditions in summer and highest aerosol concentrations in autumn and winter. Transport paths of air masses at cloud level were determined using back trajectories. Air mass characteristics showed lowest ground-level concentrations in marine conditions and highest ground-level concentrations in continental conditions, as expected.

Cloud properties were classified according to prevailing cloud level air mass and season. Cloud base and top altitudes were highest in summer and lowest in spring. Clouds in marine-modified air masses were the highest, and cloud base altitudes were lowest in continental modified air. Cloud depth was slightly larger in autumn and winter than in spring and summer. Mainly, marine and marine-modified air masses were observed in summer, although the largest number of data points were obtained in this season. In summer, continental air masses transported from Europe were probably characterized by thermodynamic conditions less favorable for the formation of the stratiform clouds that were investigated here. Aerosol concentrations were lowest during summer, which agreed well with the observed air mass types.

The results presented here confirm the theory and previous findings of higher CDNC and lower r_{eff} with greater pollution. It is important to validate such theories on a statistically significant scale, as was done by using the large data set presented here. Generally, the median CDNC ranged from 60 cm^{-3} in marine air masses to 160 cm^{-3} in continental air. The median r_{eff} ranged from 8 μm in continental modified air to 10 μm in marine air. Droplet size distributions were broader in marine cases and narrower in continental cases. Overall, COT and albedo were lower in cleaner air masses and higher in more polluted conditions, with medians of 2.1 and 4.9, and 0.22 and 0.39, respectively. However, the calculations of COT and albedo were strongly affected by the observed LWP and resulting subadiabaticity.

Comparison of SYRSOC results with MODIS observations showed a moderate correlation of r_{eff} ($R^2 = 0.43$) and a rather poor agreement of COT ($R^2 = 0.19$). No correlation was found between the integrated SYRSOC LWC and MODIS CWP due to SYRSOC drizzle screening. Agreement was improved by rerunning SYRSOC without drizzle screening, thus changing R^2 of LWC from 0.04 to 0.14. Comparison of r_{eff} with drizzle resulted in a slope near 1 and a small offset of −1 μm.

This study ties together large data sets of multiple ground-based and satellite-borne sensors, using sophisticated analysis tools, in order to obtain thorough insights into cloud characteristics. It investigated cloud microphysical properties under the influence of different air masses and, hence, different aerosol types and concentrations. The number of cases spread over a period of more than 6 years, allowed a statistically sound interpretation of the results. Generally, this work confirms findings from case studies [*Miles et al.*, 2000; *Martucci and O'Dowd*, 2011] and model studies [*Rémillard et al.*, 2013]. Additionally, application of the method on such a large scale contributes to the understanding of processes and effects of aerosol-cloud interactions.

Acknowledgments

The authors would like to thank the Irish Environmental Protection Agency (EPA) for fellowship 2012-CCRP-FS.13 and acknowledge support through HEA (Higher Education Authority)PRTLI4. Besides, we gratefully acknowledge the NOAA Air Resources Laboratory (ARL) for provision of the HYSPLIT transport and dispersion model. This work benefits from involvement in Cloudnet; European Research Infrastructure for the observation of Aerosol, Clouds, and Trace gases ACTRIS and ACTRIS-2 (grant agreement numbers 262254 and 654109); European FP7 collaborative project BACCHUS (Impact of Biogenic versus Anthropogenic emissions on Clouds and Climate: towards a Holistic UnderStanding, grant agreement number 603445); and COST actionES1303: TOPROF (Towards operational ground based profiling with ceilometers, doppler lidars and microwave radiometers for improving weather forecasts) supported by COST (European Cooperation in Science and Technology). We acknowledge the Terra and Aqua mission scientists and associated NASA personnel for production and provision of MODIS data. SYRSOC results for the 118 cloud cases are published in netcdf format under http://doi.org/10.5281/zenodo.154137.

References

Albrecht, B. A. (1989), Aerosols, cloud microphysics, and fractional cloudiness, *Science*, *245*, 1227–1230, doi:10.1126/science.245.4923.1227.

Bauer-Pfundstein, M. R., and U. Goersdorf (2007), Target separation and classification using cloud radar Doppler-spectra, paper presented at 33rd Conference on Radar Meteorology, p. 11B.2, Cairns Queensland, 6–10 Aug.

Boers, R., H. Russchenberg, J. Erkelens, and V. Venema (2000), Ground-based remote sensing of stratocumulus properties during CLARA, 1996, *J. Appl. Meteorol.*, *39*, 169–181, doi:10.1175/1520-0450(2000)039<0169:GBRSOS>2.0.CO;2.

Boucher, O., et al. (2013), Clouds and aerosols, in *Climate Change 2013: The Physical Science Basis. Contribution of Working Group I to the Fifth Assessment Report of the Intergovernmental Panel on Climate Change*, edited by T. F. Stocker et al., pp. 571–657, Cambridge Univ. Press, Cambridge, U. K., and New York.

Brandau, C. L., H. W. J. Russchenberg, and W. H. Knap (2010), Evaluation of ground-based remotely sensed liquid water cloud properties using shortwave radiation measurements, *Atmos. Res.*, *96*, 366–377, doi:10.1016/j.atmosres.2010.01.009.

Brenguier, J.-L., H. Pawlowska, and L. Schüller (2003), Cloud microphysical and radiative properties for parameterization and satellite monitoring of the indirect effect of aerosol on climate, *J. Geophys. Res.*, *108*(D15), 8632, doi:10.1029/2002JD002682.

Brenguier, J.-L., F. Burnet, and O. Geoffroy (2011), Cloud optical thickness and liquid water path does the *k* coefficient vary with droplet concentration?, *Atmos. Chem. Phys.*, *11*, 9771–9786, doi:10.5194/acp-11-9771-2011.

Ceburnis, D., M. Rinaldi, J. Keane-Brennan, J. Ovadnevaite, G. Martucci, L. Giulianelli, and C. D. O'Dowd (2014), Marine submicron aerosol sources, sinks and chemical fluxes, *Atmos. Chem. Phys. Discuss.*, *14*, 23,847–23,889, doi:10.5194/acpd-14-23847-2014.

Coakley, S. A., and W. M. Angevine (2002), Boundary layer height and entrainment zone thickness measured by lidars and wind-profiling radars, *J. Appl. Meteorol.*, *39*, 1233–1247.

Comstock, K. K., R. Wood, S. E. Yuter, and C. S. Bretherton (2004), Reflectivity and rain rate in and below drizzling stratocumulus, *Q. J. R. Meteorol. Soc.*, *130*, 2891–2918, doi:10.1256/qj.03.187.

Crewell, S., and U. Löhnert (2003), Accuracy of cloud liquid water path from ground-based microwave radiometry 2. Sensor accuracy and synergy, *Radio Sci.*, *38*(3), 8042, doi:10.1029/2002RS002634.

Dall'Osto, M., et al. (2010), Aerosol properties associated with air masses arriving into the North East Atlantic during the 2008 Mace Head EUCAARI intensive observing period: An overview, *Atmos. Chem. Phys.*, *10*, 8413–8435, doi:10.5194/acp-10-8413-2010.

Draxler, R. R., and G. D. Rolph (2014), *HYSPLIT (HYbrid Single-Particle Lagrangian Integrated Trajectory) Model access via NOAA ARL READY Website*, NOAA Air Resour. Lab., Silver Spring, Md. [Available at http://ready.arl.noaa.gov/HYSPLIT.php.]

Ferek, R. J., et al. (2000), Drizzle suppression in ship tracks, *J. Atmos. Sci.*, *57*, 2707–2728, doi:10.1175/1520-0469(2000)057<2707:DSIST>2.0.CO;2.

Fox, N. I., and A. J. Illingworth (1997), The retrieval of stratocumulus cloud properties by ground-based cloud radar, *J. Appl. Meteorol.*, *36*, 485–492, doi:10.1175/1520-0450(1997)036<0485:TROSCP>2.0.CO;2.

Heese, B., H. Flentje, D. Althausen, A. Ansmann, and S. Frey (2010), Ceilometer lidar comparison: Backscatter coefficient retrieval and signal-to-noise ratio determination, *Atmos. Meas. Tech.*, *3*, 1763–1770, doi:10.5194/amt-3-1763-2010.

Hudson, J. G. (1993), Cloud condensation nuclei, *J. Appl. Meteorol.*, *32*, 596–607, doi:10.1175/1520-0450(1993)032<0596:CCN>2.0.CO;2.

Hudson, J. G., and S. S. Yum (1997), Droplet spectral broadening in marine stratus, *J. Atmos. Sci.*, *54*, 2642–2654, doi:10.1175/1520-0469(1997)054<2642:DSBIMS>2.0.CO;2.

Hudson, J. G., and S. S. Yum (2001), Maritime-continental drizzle contrasts in small cumuli, *J. Atmos. Sci.*, *58*, 915–926, doi:10.1175/1520-0469(2001)058<0915:MCDCIS>2.0.CO;2.

Hudson, J. G., S. Noble, V. Jha, and S. Mishra (2009), Correlations of small cumuli droplet and drizzle drop concentrations with cloud condensation nuclei concentrations, *J. Geophys. Res.*, *114*, D05201, doi:10.1029/2008JD010581.

Illingworth, A. J., et al. (2007), Cloudnet—Continuous evaluation of cloud profiles in seven operational models using ground-based observations, *Bull. Am. Meteorol. Soc.*, *88*, 883–898, doi:10.1175/BAMS-88-6-883.

Jennings, S. G., M. Geever, F. M. McGovern, J. Francis, T. G. Spain, and T. Donaghy (1997), Microphysical and physio-chemical characterization of atmospheric marine and continental aerosol at Mace Head, *Atmos. Environ.*, *31*, 2795–2808, doi:10.1016/S1352-2310(97)00039-3.

Jennings, S. G., C. Kleefeld, C. D. O'Dowd, C. Junker, T. G. Spain, P. O'Brien, A. F. Roddy, and T. C. O'Connor (2003), Mace Head Atmospheric Research Station—Characterization of aerosol radiative parameters, *Boreal Environ. Res.*, *8*, 303–314.

Lacis, A. A., and J. E. Hansen (1974), A parameterization for the absorption of solar radiation in the Earth's atmosphere, *J. Atmos. Sci.*, *31*, 118–133, doi:10.1175/1520-0469(1974)031<0118:APFTAO>2.0.CO;2.

Lance, S., J. Medina, J. N. Smith, and A. Nenes (2006), Mapping the operation of the DMT continuous flow CCN counter, *Aerosol Sci. Technol.*, *40*, 1–13, doi:10.1080/02786820500543290.

Lohmann, U., and J. Feichter (2005), Global indirect aerosol effects: A review, *Atmos. Chem. Phys.*, *5*, 715–737, doi:10.5194/acp-5-715-2005.

Löhnert, U., and S. Crewell (2003), Accuracy of cloud liquid water path from ground-based microwave radiometry 1. Dependency on cloud model statistics, *Radio Sci.*, *38*(3), 8041, doi:10.1029/2002RS002654.

Löhnert, U., D. D. Turner, and S. Crewell (2009), Ground-based temperature and humidity profiling using spectral infrared and microwave observations. Part I: Simulated retrieval performance in clear-sky conditions, *J. Appl. Meteorol. Climatol.*, *48*, 1017–1032, doi:10.1175/2008JAMC2060.1.

Martucci, G., and C. D. O'Dowd (2011), Ground-based retrieval of continental and marine warm cloud microphysics, *Atmos. Meas. Tech.*, *4*, 2749–2765, doi:10.5194/amt-4-2749-2011.

Martucci, G., C. Milroy, and C. D. O'Dowd (2010), Detection of cloud base height using Jenoptik CHM15K and Vaisala CL31 ceilometers, *J. Atmos. Oceanic Technol.*, *27*, 305–318, doi:10.1175/2009JTECHA1326.1.

Martucci, G., J. Ovadnevaite, D. Ceburnis, H. Berresheim, S. Varghese, D. Martin, R. Flanagan, and C. D. O'Dowd (2012), Impact of volcanic ash plume aerosol on cloud microphysics, *Atmos. Environ.*, *48*, 205–218, doi:10.1016/j.atmosenv.2011.12.033.

Martucci, G., C. Milroy, K. Bower, M. Gallagher, G. Lloyd, and C. D. O'Dowd (2013), Comparison of in-situ, satellite and ground-based remote sensing retrievals of liquid cloud microphysics during MACLOUD,paper presented at 19th International Conference on Nucleation and Atmospheric Aerosols and Nucleation Symposium, AIP Conference, vol. 1527, pp. 828–831, Fort Collins, Colo., 23–28 Jun., doi:10.1063/1.4803399.

Melchionna, S., M. Bauer, and G. Peters (2008), A new algorithm for the extraction of cloud parameters using multipeak analysis of cloud radar data: First application and results, *Meteorol. Z.*, *17*, 613–620, doi:10.1127/0941-2948/2008/0322.

Miles, N. L., J. Verlinde, and E. E. Clothiaux (2000), Cloud droplet size distributions in low-level stratiform clouds, *J. Atmos. Sci.*, *57*, 295–311, doi:10.1175/1520-0469(2000)057<0295:CDSDIL>2.0.CO;2.

Mulcahy, J. P., C. D. O'Dowd, S. G. Jennings, and D. Ceburnis (2008), Significant enhancement of aerosol optical depth in marine air under high wind conditions, *Geophys. Res. Lett.*, *35*, L16810, doi:10.1029/2008GL034303.

Noble, S. R., and J. G. Hudson (2015), MODIS comparisons with northeastern Pacific in situ stratocumulus microphysics, *J. Geophys. Res. Atmos.*, *120*, 8332–8344, doi:10.1002/2014JD022785.

O'Connor, T. C., S. G. Jennings, and C. D. O'Dowd (2008), Highlights from 50 years of aerosol measurements at Mace Head, *Atmos. Res.*, *90*, 338–355, doi:10.1016/j.atmosres.2008.08.014.

O'Dowd, C., D. Ceburnis, J. Ovadnevaite, A. Vaishya, M. Rinaldi, and M. C. Facchini (2014), Do anthropogenic, continental or coastal aerosol sources impact on a marine aerosol signature at Mace Head?, *Atmos. Chem. Phys.*, *14*, 10,687–10,704, doi:10.5194/acp-14-10687-2014.

O'Dowd, C. D., J. A. Lowe, and M. H. Smith (1999), Coupling sea-salt and sulphate interactions and its impact on cloud droplet concentration predictions, *Geophys. Res. Lett.*, *26*, 1311–1314, doi:10.1029/1999GL900231.

Ovadnevaite, J., D. Ceburnis, G. Martucci, J. Bialek, C. Monahan, M. Rinaldi, M. C. Faccini, H. Berresheim, D. R. Worsnop, and C. O'Dowd (2011), Primary marine organic aerosol: A dichotomy of low hygroscopicity and high CCN activity, *Geophys. Res. Lett.*, *38*, L21806, doi:10.1029/2011GL048869.

Ovadnevaite, J., D. Ceburnis, M. Canagaratna, H. Berresheim, J. Bialek, G. Martucci, D. R. Worsnop, and C. O'Dowd (2012), On the effect of wind speed on submicron sea salt mass concentrations and source fluxes, *J. Geophys. Res.*, *117*, D16201, doi:10.1029/2011JD017379.

Ovadnevaite, J., D. Ceburnis, S. Leinert, M. Dall'Osto, M. Canagaratna, S. O'Doherty, H. Berresheim, and C. O'Dowd (2014), Submicron NE Atlantic marine aerosol chemical composition and abundance: Seasonal trends and air mass categorization, *J. Geophys. Res. Atmos.*, *119*, 11,850–11,863, doi:10.1002/2013JD021330.

Pierce, J. R., and P. J. Adams (2006), Global evaluation of CCN formation by direct emission of sea salt and growth of ultrafine sea salt, *J. Geophys. Res.*, *111*, D06203, doi:10.1029/2005JD006186.

Platnick, S., et al. (2015a), *MODIS/Terra Level-2 (L2) Cloud Product (06_L2)*, NASA MODIS Adaptive Processing System, Goddard Space Flight Center, U.S.A., doi:10.5067/MODIS/MOD06_L2.006.

Platnick, S., et al. (2015b), *MODIS/Aqua Level-2 (L2) Cloud Product (06_L2)*, NASA MODIS Adaptive Processing System, Goddard Space Flight Center, U.S.A., doi:10.5067/MODIS/MYD06_L2.006.

Probert-Jones, J. R. (1962), The radar equation in meteorology, *Q. J. R. Meteorol. Soc.*, *88*, 485–495, doi:10.1002/qj.49708837810.

Reade, L., S. G. Jennings, and G. McSweeney (2006), Cloud condensation nuclei measurements at Mace Head, Ireland, over the period 1994-2002, *Atmos. Res.*, *82*, 610–621, doi:10.1016/j.atmosres.2006.02.017.

Rémillard, J., P. Kollias, and W. Szyrmer (2013), Radar-radiometer retrievals of cloud number concentration and dispersion parameter in nondrizzling marine stratocumulus, *Atmos. Meas. Tech.*, *6*, 1817–1828, doi:10.5194/amt-6-1817-2013.

Rosenfeld, D., U. Lohmann, G. B. Raga, C. D. O'Dowd, M. Kulmala, S. Fuzzi, A. Reissell, and M. O. Andreae (2008), Flood or drought: How do aerosols affect precipitation?, *Science*, *321*, 1309–1313, doi:10.1126/science.1160606.

Sauvageot, H., and J. Omar (1987), Radar reflectivity of cumulus clouds, *J. Atmos. Oceanic Technol.*, *4*, 264–272, doi:10.1175/1520-0426(1987)004<0264:RROCC>2.0.CO;2.

Squires, P. (1958), The microstructure and colloidal stability of warm clouds: Part I—The relation between structure and stability, *Tellus A*, *10*, 256–261.

Stephens, G. L., et al. (2002), The CloudSat mission and the A-train—A new dimension of space-based observations of clouds and precipitation, *Bull. Am. Meteorol. Soc.*, *83*, 1771–1790, doi:10.1175/BAMS-83-12-1771.

Twomey, S. (1974), Pollution and the planetary albedo, *Atmos. Environ.*, *8*, 1251–1256, doi:10.1016/0004-6981(74)90004-3.

Twomey, S. (1977), The influence of pollution on shortwave albedo of clouds, *J. Atmos. Sci.*, *34*, 1149–1152, doi:10.1175/1520-0469(1977)034<1149:TIOPOT>2.0.CO;2.

Vong, R. J., and D. S. Covert (1998), Simultaneous observations of aerosol and cloud droplet size spectra in marine stratocumulus, *J. Atmos. Sci.*, *55*, 2180–2192, doi:10.1175/1520-0469(1998)055<2180:SOOAAC>2.0.CO;2.

Winker, D. M., W. H. Hunt, and M. J. McGill (2007), Initial performance assessment of CALIOP, *Geophys. Res. Lett.*, *34*, L19803, doi:10.1029/2007GL030135.

Yoon, Y. J., et al. (2007), Seasonal characteristics of the physicochemical properties of North Atlantic marine atmospheric aerosols, *J. Geophys. Res.*, *112*, D04206, doi:10.1029/2005JD007044.

Yum, S. S., and J. G. Hudson (2002), Maritime/continental microphysical contrasts in stratus, *Tellus B*, *54*, 61–73, doi:10.1034/j.1600-0889.2002.00268.x.

Zuidema, P., E. R. Westwater, C. Fairall, and D. Hazen (2005), Ship-based liquid water path estimates in marine stratocumulus, *J. Geophys. Res.*, *110*, D20206, doi:10.1029/2005JD005833.